

# Chemical Science

Accepted Manuscript

This article can be cited before page numbers have been issued, to do this please use: A. Serez, F. Aleotti, P. Gerbaux, L. Muccioli and J. Cornil, *Chem. Sci.*, 2026, DOI: 10.1039/D6SC01578F.



This is an Accepted Manuscript, which has been through the Royal Society of Chemistry peer review process and has been accepted for publication.

Accepted Manuscripts are published online shortly after acceptance, before technical editing, formatting and proof reading. Using this free service, authors can make their results available to the community, in citable form, before we publish the edited article. We will replace this Accepted Manuscript with the edited and formatted Advance Article as soon as it is available.

You can find more information about Accepted Manuscripts in the [Information for Authors](#).

Please note that technical editing may introduce minor changes to the text and/or graphics, which may alter content. The journal's standard [Terms & Conditions](#) and the [Ethical guidelines](#) still apply. In no event shall the Royal Society of Chemistry be held responsible for any errors or omissions in this Accepted Manuscript or any consequences arising from the use of any information it contains.

Cite this: DOI: 00.0000/xxxxxxxxxx

# Mechanistic Insights into Azo Compound Back-Isomerization from Spin-Flip Time-Dependent DFT combined to Marcus Theory

Ari Serez,<sup>a,b</sup> Flavia Aleotti,<sup>c</sup> Pascal Gerbaux,<sup>b</sup> Luca Muccioli,<sup>c</sup> and Jérôme Cornil<sup>\*a</sup>Received Date  
Accepted Date

DOI: 00.0000/xxxxxxxxxx

Interest in photosensitive molecules has increased significantly over the past decade, with particular attention given to photoswitchable systems. Among these, azobenzene stands out as a reference compound due to its broad range of applications, in particular for solar energy storage. While the trans-to-cis photoisomerization has been relatively well characterized, the reverse cis-to-trans isomerization remains a complex process potentially involving multi-state physics. In this study, we compile recent theoretical advances aimed at modeling this process and introduce, through the spin-flip time-dependent density functional theory (SF-TDDFT) approach combined to the semi-classical Marcus equation, a fast and efficient method to investigate the mechanisms of thermal back-isomerization of azo derivatives. By comparing various exchange–correlation functionals with CASPT2 reference data, we demonstrate that the PBE0(D3BJ) functional provides an accurate description for the non-adiabatic rotational pathway. We successfully reproduce the experimental values (88.6 vs. 88.3  $\text{kJ/mol}$  for the experimental enthalpy of activation, and -53.0 vs. -50.2  $\text{J/mol} \cdot \text{K}$  for the experimental entropy of activation) for azobenzene, thus motivating the extension of this methodology to other azo derivatives. This approach can be further generalized to a broader class of azo-based photo-switches in future studies.

## 1 Introduction

Modern society faces numerous energy-related challenges, especially in the transition from fossil fuels to renewable energy sources. To this end, many technologies have been developed, such as solar panels to produce electricity, and batteries to store it. To avoid inherent charge losses, an interesting new approach relies on the storage of energy into chemical structures. To do so, photo-switchable molecules that can isomerize by capturing a photon from the sun are used. A metastable isomer is then created, in which the solar energy is stored; this is referred to as a MOlecular Solar Thermal (MOST) system. This technology has been widely studied over the last decade<sup>1–3</sup>. Among the various existing photochromic systems, azobenzene and derivatives appear as very promising.<sup>1,4–6</sup> Azobenzene can photo-isomerize

from a trans (E) stable isomer to a cis (Z) metastable isomer, see Figure 1. These compounds offer many advantages, such as a low production cost, a high photo-isomerization quantum yield (44 %), a large half-lifetime of the metastable form (about 4 days) and a decent storage energy density (0.20  $\text{MJ/kg}$ , or 36  $\text{kJ} \cdot \text{mol}^{-1}$ )<sup>7</sup>. The photo-isomerization, which can be considered as the chemical analogue of the charging process in a battery, has been extensively studied<sup>1,4,8</sup>. However, the thermal back-isomerization, which can be considered as the discharging process, has been largely overlooked. To the best of our knowledge, only a few studies have focused on this process<sup>9–14</sup>. It is commonly accepted that the thermal back-isomerization can occur via two distinct mechanisms; the first involves the opening of the NNC angle, referred to as the inversion mechanism, while the second one proceeds via a rotation of a phenyl group around the double bond between the two nitrogen atoms and is referred to as the rotation mechanism (Figure 1).

The minimum energy reaction path (MERP) was typically searched by DFT calculations, to describe the inversion mechanism.<sup>15</sup> However, an inconsistency was pointed out recently: the activation entropy,  $\Delta^\ddagger S$ , is calculated to be positive (about +10  $\text{J} \cdot \text{mol}^{-1} \cdot \text{K}^{-1}$ ) at the DFT level against a negative experimental value for azobenzene (about -50.2  $\text{J} \cdot \text{mol}^{-1} \cdot \text{K}^{-1}$ )<sup>16,17</sup>. The ex-

<sup>a</sup> Laboratory for Chemistry of Novel Materials, University of Mons, Place du Parc 23, 7000 Mons, Belgium. E-mail: Jerome.Cornil@umons.ac.be

<sup>b</sup> Organic Synthesis and Mass Spectrometry Laboratory, University of Mons, Place du Parc 23, 7000 Mons, Belgium

<sup>c</sup> Dipartimento di Chimica Industriale "Toso Montanari", University of Bologna, Via Gobetti 85, 40129 Bologna, Italy

† Supplementary Information available: Benchmark of SF-TDDFT functionals, transmission coefficient derived from Marcus, details on Marcus-Levich-Jortner and mechanistic details on azothiophene derivatives. See DOI: 00.0000/00000000.



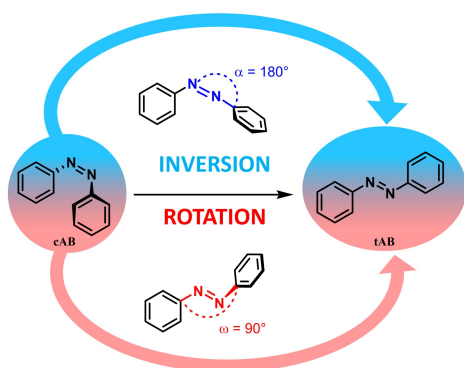


Fig. 1 Reaction pathways for the back isomerization mechanism.  $\alpha$  (in blue) is the NNC bending angle involved in the inversion, and  $\omega$  (in red) is the dihedral angle involved in the rotation.

perimental rate constant was well reproduced from a standard Eyring theory based on molecular parameters calculated at the DFT level, whereas Hartree-Fock and post-HF methods (such as MP2) were not able to provide the right order of magnitude<sup>17</sup>. This discrepancy on the sign and amplitude of  $\Delta^\ddagger S$ , known as the “entropy puzzle”, was studied recently in detail by Reimann and coworkers<sup>10</sup>. Their highly correlated calculations suggest that the actual mechanism for the thermal back-isomerization of azobenzene is not an inversion but is rather based on a multi-state rotational process. Instead of a classical chemical reaction occurring on a single potential energy surface (PES), it was found that the lowest triplet state,  $T_1$ , intersects with the ground state,  $S_0$  (Figure 2). Estimating the rate constant thus requires accounting for a possible transition between these two states if the intersystem crossing is sufficiently fast (in other words, a non-adiabatic transition state description). The importance of the  $T_1$  state was supported experimentally by observing, in a few instances, an external heavy-atom effect on the kinetics of back-isomerization.<sup>10,13</sup> Since the mixing between singlet and triplet states involves a spin-orbit coupling, adding heavy elements is expected to enhance this coupling, which is proportional to the fourth power of the nuclear charge.<sup>18</sup>

The electronic nature of this triplet state can be understood from a simple molecular orbital representation. During the rotation, the azo- $\pi$  bond is broken since the  $2p_z$  orbitals of each nitrogen do not longer overlap, which can promote a biradical form either in a singlet or triplet state. According to Hund's rule, the lowest triplet state will be lower in energy than the lowest singlet state at  $90^\circ$ , as represented on Figure 2. A drawback of DFT is that it fails to locate a transition state for the rotation mechanism by systematically converging to the transition state associated to the inversion mechanism<sup>10,13</sup>. A possibility to overcome this problem is to perform a constrained optimization by freezing the NNC angles.<sup>14</sup> This discrepancy was explained by the fact that the ground state and the first singlet excited state  $S_1$  mix near  $90^\circ$ : this mixing can be quantitatively described only with multi-reference methods, or at least with a method that can capture the multi-configurational physics of the problem.<sup>10</sup> A quasi-exact value for the activation entropy

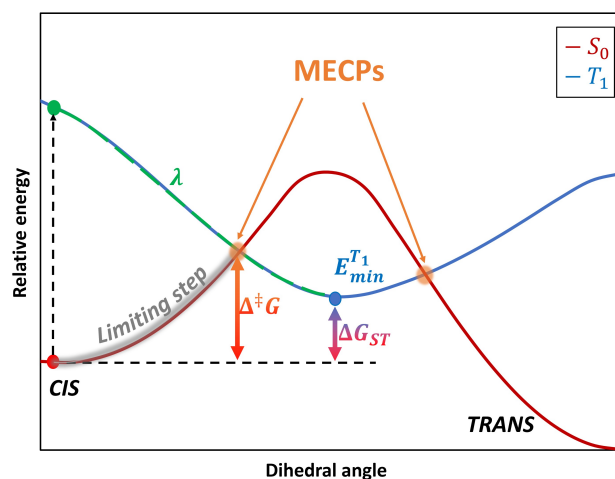


Fig. 2 Schematic representation of the electronic states involved in the actual minimum energy reaction path. The  $S_0$  and  $T_1$  are represented as red and blue curves respectively. MECP stands for Minimum-Energy Crossing-Point. The limiting step considered in this study is highlighted in grey. Parameters entering into the WKB and Marcus rate equations are displayed on the scheme, *i.e.*  $\lambda$ ,  $\Delta^\ddagger G$ , and  $\Delta G_{ST}$ .

can thus be recovered by combining highly-correlated methods to a formalism taking into account the amplitude of the spin orbit coupling at the crossing of the  $S_0$  and  $T_1$  states, such as the semi-classical Wentzel-Kramers-Brillouin (WBK) theory.<sup>10</sup>

In order to efficiently explore the vast chemical space of potential MOST candidates, there is a need to reduce the computational effort while maintaining a good level of accuracy. In the search of an alternative approach to the coupling of highly-correlated methods to the WBK theory used in Ref<sup>10</sup>, the present work aims at investigating the relevance of coupling the results of spin-flip(SF) TD-DFT calculations with the WBK theory. SF-TDDFT is currently emerging as a fast and accurate method to be used in the presence of a conical intersection or to deal with a ground state whose wave-function cannot be simply represented with a single determinant.<sup>19</sup> A secondary aim is to assess whether the use of the semi-classical Marcus theory to describe the limiting kinetic step can provide rates similar to those obtained with WBK. It must be noted that Marcus theory has already been used to compute the rate of intersystem crossing processes by relying on three easily accessible molecular parameters (*i.e.*, the reorganization energy, the spin-orbit coupling, and the free energy of the reaction). This approach will be first applied to the prototypical azobenzene molecule and will then be extended to other systems.

## 2 Theoretical background

We have first performed a benchmark of different DFT functionals to reproduce the potential energy curves of the  $S_0$  and  $T_1$  states taking CASPT2 results as reference. We also employed the D3BJ dispersion correction, since DFT functionals usually do not correctly reproduce the inter/intramolecular van der Waals in-



teractions.<sup>20</sup> All the calculations were performed using Q-Chem 6.3 at the SF-TDDFT and DFT level and OpenMolcas 25.06 for the CASSCF/CASPT2 calculations. The spin-flip approach relies on the linear-response time-dependent DFT (LR-TDDFT) theory, which is well described by Casida's equation :

$$\begin{pmatrix} \mathbf{A} & \mathbf{B} \\ \mathbf{B}^* & \mathbf{A}^* \end{pmatrix} \begin{pmatrix} \mathbf{x}^{(n)} \\ \mathbf{y}^{(n)} \end{pmatrix} = \omega_n \begin{pmatrix} 1 & 0 \\ 0 & -1 \end{pmatrix} \begin{pmatrix} \mathbf{x}^{(n)} \\ \mathbf{y}^{(n)} \end{pmatrix} \quad (1)$$

where  $\omega$  are the excitation energies and  $\mathbf{x}$  and  $\mathbf{y}$  are vectors containing the excitation and de-excitation coefficients for each excited state. In the classical formalism of TDDFT, the reference determinant corresponds to the ground-state solution of the Kohn-Sham equation. The spin-flip approach takes as reference state a well-behaved high-spin state, typically the  $T_1$  state ( $m_S = 1$ ), such that lower-spin states (e.g. the  $S_0$  state) are recovered by a simple excitation with a spin-flip process from this high-spin reference state. In Casida's equation (Eq. 1), the  $\mathbf{A}$  and  $\mathbf{B}$  matrices have the following expression within classical TDDFT (using Mulliken's notation) :

$$A_{ia}^{jb} = \delta_{ij}\delta_{ab}(\epsilon_a - \epsilon_i) + (ia|f_H|jb) + (ia|f_{xc}|jb) \quad (2)$$

$$B_{ia}^{jb} = (ia|f_H|bj) + (ia|f_{xc}|bj) \quad (3)$$

where  $f_H$  and  $f_{xc}$  are the Hartree and exchange-correlation kernels. In presence of a spin-flip transition, the matrices  $\mathbf{A}$  and  $\mathbf{B}$  (Eq. 2 and 3) further simplify into the following form for a hybrid functional :

$$A_{ia}^{j\bar{b}} = \delta_{ij}\delta_{a\bar{b}}(\epsilon_a - \epsilon_i) - C_{HF}(ij|f_H|\bar{a}\bar{b})$$

$$B_{ia}^{j\bar{b}} = -C_{HF}(ib|f_H|\bar{a}\bar{j})$$

with  $C_{HF}$ , the fraction of exact exchange included in the hybrid functional. The upper bars indicate the  $\beta$  spin-orbitals, as in Ref<sup>19</sup>. Thus, from a single-reference formalism, we can generate a multi-configurational wavefunction that can be used to describe situations where static correlation is important, e.g. bond breaking and conical intersection.<sup>19</sup> The main problem of SF-TDDFT is that it may suffer from spin-contamination; in such a case, spin-adapted (SA) SF-TDDFT or mixed-reference (MR) SF-TDDFT can be used to significantly reduce spin-contamination. In all our calculations, the maximum spin-contamination was 0.1; this value is reasonably small, and we thus consider that it did not interfere significantly with the results.

As mentioned above, it is necessary to go beyond the Eyring transition state theory (TST) and turn to a Non-Adiabatic TST (NA-TST); this formalism has already been applied to spin-forbidden reactions.<sup>21</sup> If we consider two crossing potential energy surfaces associated to  $S_0$  and  $T_1$ , as shown in Figure 2, the hopping probability from  $S_0$  to  $T_1$  at the crossing point can be calculated from the Landau-Zener (LZ) theory as<sup>21-24</sup> :

$$p = (1 - P_{LZ})(1 + P_{LZ}) \quad (4)$$

In equation 4,  $p$  considers that the hopping from one *adiabatic*

state to another can take place along the first pass at the crossing point or at the second pass when going back to the equilibrium geometry of the initial state, and

$$P_{LZ}(\epsilon) = \exp\left(\frac{-2\pi|V_{SO}|^2}{\hbar\Delta F} \sqrt{\frac{\mu}{2(\epsilon - E_{MECP})}}\right) \quad (5)$$

$P_{LZ}$  is the Landau-Zener probability of hopping from one *adiabatic* state to another during the first pass. In equation 5,  $V_{SO}$  is the spin-orbit coupling, necessary to promote the interaction between the singlet and triplet states,  $\Delta F = |F_{S_0} - F_{T_1}|$  is the relative slope of the two surfaces at the crossing point,  $\mu$  is the reduced mass of the vibration orthogonal to the crossing seam along the hopping coordinate,  $E_{MECP}$  is the energy of the minimum-energy crossing-point (MECP), and the energy  $\epsilon$  lies in the energy gap between the two adiabatic surfaces. From this equation, the semiclassical Marcus equation (Eq. 6) can be derived by relying on the parabolic shape of the potential energy surfaces of reactants and products<sup>25</sup>:

$$k(T) = \frac{2\pi|V_{SO}|^2}{\hbar\sqrt{4\pi\lambda k_B T}} \exp\left(-\frac{(\Delta G_{ST} + \lambda)^2}{4\lambda k_B T}\right) \quad (6)$$

where  $\lambda$  is the reorganization energy accounting for the change in geometry going from the equilibrium geometry in the ground state to that in the triplet state ( $T_1$ ).  $\Delta G_{ST}$  is the free energy difference between the  $S_0$  and  $T_1$  minima. In the LZ theory, the hopping probability is equal to zero for energies below the energy of the MECP. An alternative formalism allowing for tunneling effects is to consider the following equation<sup>21,23</sup>:

$$p = 4\pi^2|V_{SO}|^2 \left(\frac{2\mu}{\hbar^2\bar{F}\Delta F}\right)^{2/3} Ai^2\left[-(\epsilon - E_{MECP})\left(\frac{2\mu\Delta F^2}{\hbar^2\bar{F}^4}\right)^{1/3}\right] \quad (7)$$

where  $Ai$  denotes the Airy function and  $\bar{F}$  is the average of the slopes. We can approximate this equation to<sup>23</sup> :

$$p = \frac{\pi^{3/2}\beta}{2\sqrt{\epsilon_0 k_B T}} \left[1 + \frac{1}{2} \exp\left(\frac{1}{12\beta^2(\epsilon_0 k_B T)^3}\right)\right] \quad (8)$$

$$\beta = \frac{4|V_{SO}|^3}{\hbar} \left(\frac{\mu}{\bar{F}\Delta F}\right)^{1/2} ; \quad \epsilon_0 = \frac{\Delta F}{2\bar{F}|V_{SO}|}$$

which is also known as the Wentzel-Kramers-Brillouin (WKB) approximation<sup>10,23</sup>. All the parameters needed ( $\mu$ ,  $\Delta F$ ,  $\bar{F}$ ) are calculated using the GLOWFreq suite<sup>26</sup>. Assuming the  $S_0 \rightarrow T_1$  crossing as the rate-determining step, we can use  $p$  from Eq. 8 as transmission coefficient,  $\gamma(T) = p$ , in Eyring equation:

$$k(T) = \gamma(T) \frac{k_B T}{h} \exp\left(-\frac{\Delta^\ddagger G}{RT}\right) \quad (9)$$

Using the definition  $\Delta^\ddagger G = \Delta^\ddagger H - T\Delta^\ddagger S$ , Eq. 9 can be transformed to obtain an equation linear in  $1/T$ :

$$\ln\left(\frac{k(T)}{T}\right) = \ln(\gamma(T)) + \ln\left(\frac{k_B}{h}\right) + \frac{\Delta^\ddagger S}{R} - \frac{\Delta^\ddagger H}{R} \frac{1}{T} \quad (10)$$

By plotting the left-hand side of equation (10) with respect to



$1/T$ , and neglecting the temperature dependence of  $\gamma(T)$ , one obtains a straight line with slope  $-\Delta^\ddagger H/R$  and intercept  $\ln \gamma + \ln \left( \frac{k_B}{h} \right) + \frac{\Delta^\ddagger S}{R}$ . This is generally known as an *Eyring plot*, and it is often used in the analysis of experimental data, with the further assumption of  $\gamma = 1$ .

However, as pointed out by Reimann *et al*<sup>10</sup>, this latest assumption is no longer valid if spin-forbidden reactions are involved, for which  $\gamma \ll 1$ . In this case, the apparent "measured" entropy  $\Delta^\ddagger \bar{S} = \Delta^\ddagger S + R \ln \gamma$  can acquire large negative values, even though the real entropy is probably small, as predicted by QM calculations<sup>14,17</sup>. Concerning the non-adiabatic rotation mechanism, we computed  $\Delta^\ddagger G$ , which corresponds to the free energy difference between the cis isomer and the MECP, and obtained  $\Delta^\ddagger H$  and  $\Delta^\ddagger S$  from an Eyring plot (Eq. 10). For the adiabatic rotation and inversion mechanisms, in absence of intersystem crossing between the  $S_0$  and  $T_1$  states,  $\Delta^\ddagger H$  and  $\Delta^\ddagger S$  were directly obtained from frequency calculations at the cis and transition state geometries.

The spin-orbit coupling (SOC),  $V_{SO}$  in Eq. 6 and 8, is a relativistic interaction between the spin angular momentum and the orbital angular momentum of an electron. This interaction is described by the Breit-Pauli Spin-Orbit operator, as implemented in Q-Chem 6.3<sup>18,27</sup>:

$$\hat{H}_{SO}^{BP} = \frac{1}{2m_e^2 c^2} \sum_i \sum_I \frac{Z_I}{r_{iI}^3} (\hat{\mathbf{r}}_{iI} \times \hat{\mathbf{p}}_i) \cdot \hat{\mathbf{s}}_i \quad (11)$$

$$- \frac{1}{2m_e^2 c^2} \sum_i \sum_{i \neq j} \frac{1}{r_{ij}^3} (\hat{\mathbf{r}}_{ij} \times \hat{\mathbf{p}}_i) \cdot (\hat{\mathbf{s}}_i + 2\hat{\mathbf{s}}_j) \quad (12)$$

where  $i$  and  $j$  are the labels for electrons,  $Z_I$  is the charge of the nucleus  $I$ ,  $m_e$  is the electron mass, and  $c$  the speed of light. The first term (Eq. 11) corresponds to the one-electron part, which is the interaction of the spin of the electron with its orbital angular momentum. The second term (Eq. 12) is the two-electron contribution which accounts for the electron-electron interaction. In Q-Chem 6.3, the two-electron part is treated via a mean-field approach<sup>27,28</sup>.

### 3 Results and discussions

The first step in the present work was to carefully validate a functional to be used with SF-TDDFT. It has been reported that BHH-LYP is a good starting point within the spin-flip method, due to its high exchange contribution, which is important for this kind of calculation involving singlet and triplet excited states<sup>29</sup>. Nevertheless, we decided to perform a comparison of different functionals in order to find the one that best reproduces the results of the complete active space perturbation theory (CASPT2) method, i.e., a highly-correlated multi-determinant approach taken here as reference. We used the extended-multi state CASPT2 (XMS-CASPT2) formalism and the double zeta ANO-RCC-VDZP basis set with an active space (AS) of 10 electrons in 8 orbitals (Figure 3).

The AS consists of two occupied lone-pair orbitals localized on the two nitrogen atoms and all the  $\pi$  orbitals except for the two most bonding and antibonding ones. The AS was selected following the procedure proposed by Aleotti *et al.*<sup>14</sup> We performed

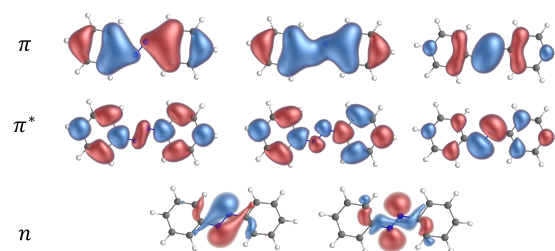


Fig. 3 Orbitals involved in the active space for the CASPT2/ANO-RCC-VDZP calculations on *trans* azobenzene.

a relaxed scan of the CNNC dihedral angle with steps of  $10^\circ$  for the ground state, and the triplet state energies were evaluated from single-point calculations at the ground state geometries. Our results are consistent with previously reported calculations<sup>9,14</sup>. We repeated the same procedure for a set of 8 DFT functionals with the 6-311G(d,p) basis set, as shown in supporting information†(Figure S1). Our approach, consisting in exploring different rungs of the Jacob's ladder in DFT, (i.e., GGA, hybrid, range-separated, etc.) showed that PBE0(D3BJ)/6-311G(d,p) calculations are those that best reproduce the ground and triplet state curves provided by the CASPT2 calculations.

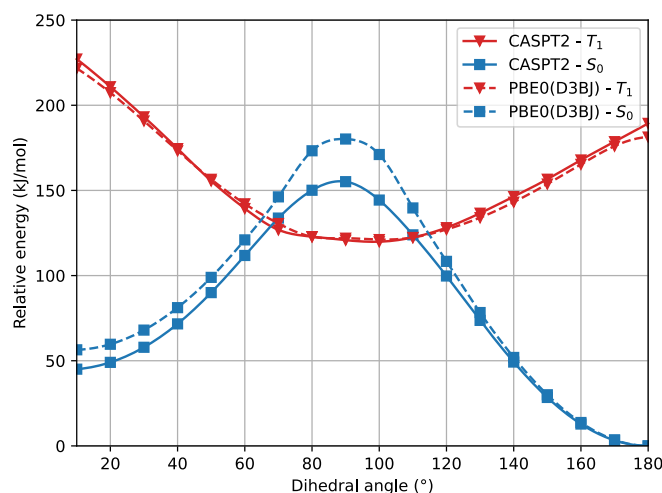


Fig. 4 Relaxed scan of the  $S_0$  and  $T_1$  states in blue squares and in red triangles, respectively. The dotted lines represent the SF-TDDFT PBE0(D3BJ) calculations and the full lines represent the CASPT2 results.

In Figure 4 we show a comparison of the relative singlet and triplet state energies as a function of the dihedral angle, for two methods, with respect to the singlet state reference energies arbitrarily set as those predicted at 180 degrees. The agreement for the triplet state is excellent at any angle, while for  $S_0$  there is a general overestimation of the energy along the pathway in the  $S_0$  state at the PBE0 level, compared to the CASPT2 results. We attribute this overestimation in part to the lack of dynamic correlation in DFT methods. Not surprisingly given the choice of our reference energies, for dihedral angles close to  $180^\circ$ , we ob-



serve that the energy difference between CASPT2 and SF-TDDFT curves is very small, with a mean value of c.a.  $1.5 \text{ kJ} \cdot \text{mol}^{-1}$  for angles ranging from  $130^\circ$  to  $180^\circ$ . Instead, the discrepancy is larger around the cis form: for angles between  $10^\circ$  and  $60^\circ$ , the deviation is about  $10 \text{ kJ} \cdot \text{mol}^{-1}$  while for angles between  $70^\circ$ - $110^\circ$ , the deviation amounts to  $18 \text{ kJ} \cdot \text{mol}^{-1}$ . This large deviation probably occurs because, at these angles, the two phenyl rings are very close to each other, a situation where electron correlation is expected to be more important. To further validate this hypothesis, we examined how the ground state energy curve is affected by the perturbation theory treatment by comparing CASSCF versus CASPT2 results; in CASPT2 calculations, the dynamic correlation is recovered by perturbation theory, exactly in the same way as in the Møller-Plesset approach at the second order (MP2 - perturbation theory applied to a HF single-reference wavefunction). Notably, the correlation energy accounts for only 0.33% of the total energy, which is consistent with the validity of a perturbative treatment, where the perturbation is expected to remain small. Figure 5 clearly shows that the PBE0(D3BJ) potential energy curve lies between the CASSCF and CASPT2 curves, indicating that the recovery of dynamic electron correlation plays a significant role. In purple, we report the correlation energy with respect to the trans isomer, for which the correlation energy is minimal: the curve peaks at  $90^\circ$ , showing that dynamic correlation is most significant at this dihedral angle, reaching a value of  $50 \text{ kJ/mol}$ , which is not negligible.

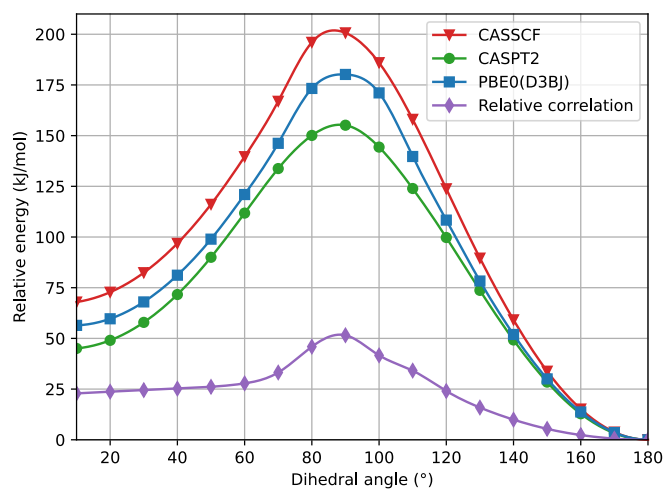


Fig. 5 Torsional energy curve of the  $S_0$  state with CASSCF (red line, with triangles), CASPT2 (green line, with dots) and PBE0(D3BJ) at the SF-TDDFT level of theory (blue line, with squares). The purple line with diamonds corresponds to the correlation energy relative to the lowest value, which is at  $180^\circ$ . The CASSCF energy is calculated at the CASPT2 relaxed geometry.

We have discussed so far the rotation mechanism, which is commonly assumed to be the minimum-energy reaction path. For completeness, we also analyzed the energy profile associated to the inversion mechanism. From Figure 6, it is clear that standard DFT and the spin-flip approach give very similar results,

which is in agreement with the hypothesis that the inversion path can be described with a single-reference method. Using the Møller-Plesset second-order perturbation theory (MP2) as reference method, our DFT approach underestimates the activation barrier mostly near the transition state. However, CASPT2 results appear to be in a better agreement with DFT (see Table 1).

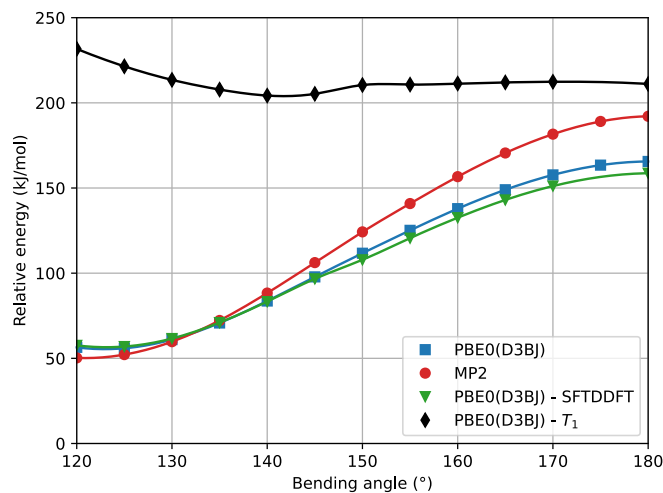


Fig. 6 Pathway of the Z→E inversion mechanism following the bending angle NNC at different levels of theory. The basis set used for the MP2 calculations is cc-pVTZ.

The next step is to determine the activation parameters, i.e.  $\Delta^\ddagger H$  and  $\Delta^\ddagger S$ , of the back-isomerization process. There are thus three possible paths: the inversion mechanism, the purely ground state rotation mechanism, and the rotation mechanism combined to a spin-forbidden transition into the  $T_1$  state. The latter was referred to as non-adiabatic rotation in a recent article<sup>30</sup>. Regarding the non-adiabatic rotation, using the WKB approximation (Eq. 8) fed by the results of highly-correlated CCSD calculations, Reimann et al found theoretical values in really good quantitative agreement with the experiment<sup>10</sup>; however, CCSD is still a single-reference method, which implies that it will suffer from same the cusp problem as normal DFT (lack of strong correlation) when the dihedral angle is around  $90^\circ$ . We also employed equation 8 and found a nice match between the values in reference<sup>10</sup> and ours (see Table 1) when injecting parameters obtained at the spin-flip PBE0(D3BJ) level, and in particular a negative value for the entropy of activation ( $-32 \text{ J} \cdot \text{mol}^{-1} \cdot \text{K}^{-1}$ ), strengthening the idea that its sign can be associated with a spin-forbidden process<sup>21</sup>. The larger the spin-orbit coupling, the more pronounced these spin-forbidden effects become; azobenzene exhibits a spin-orbit coupling of approximately  $15 \text{ cm}^{-1}$ , which is relatively large compared to typical organic conjugated systems<sup>31</sup>. This coupling was calculated at the MECF geometry. Regarding the adiabatic rotation and inversion pathways, we evaluated the activation enthalpy and entropy based on frequency calculations by determining the partition function<sup>32</sup> in the ground and transition state geometry. From the comparison of WKB enthalpies, entropies and rates with experimental ones (Table 1), it is clear that this ap-



proach performs well in describing the non-adiabatic rotational mechanism. Indeed, it yields the correct order of magnitude for the rate constant (order of  $10^{-5} s^{-1}$ ) and provides activation parameters that are consistent with experimental data as well as with other theoretical methods. However, when the Marcus equation, as formulated in Eq. 6, is applied (Table 1), although the activation entropy is well reproduced, it shows a significant discrepancy in the activation enthalpy (59.3 vs. 90.2  $kJ \cdot mol^{-1}$ ). This inaccuracy originates from the  $\Delta G_{ST}$  term: a more detailed analysis of the two key parameters in the Marcus equation - namely the reorganization energy  $\lambda$  and  $\Delta G_{ST}$ , the free-energy difference between the triplet and singlet minima - reveals that the reorganization energy is in good agreement with the CASPT2 calculations. In contrast, the energy of the *cis* isomer is overestimated at the DFT level, leading to an incorrect estimation of  $\Delta G_{ST}$ .

In Marcus equation,  $\Delta G_{ST}$  and  $\lambda$  are employed to estimate the transition state energy without actually measuring or calculating it directly with quantum chemistry methods:

$$\Delta^\ddagger G = \frac{(\Delta G_{ST} + \lambda)^2}{4\lambda} \quad (13)$$

This formula further assumes that both potential energy surfaces are perfect parabolas with the same curvature, which is not necessarily the case. We have here adopted an alternative formulation of Eq. 6:

$$k(T) = \frac{2\pi |V_{SO}|^2}{\hbar \sqrt{4\pi \lambda k_B T}} \cdot \exp\left(-\frac{\Delta^\ddagger G}{k_B T}\right) \quad (14)$$

in which, while retaining the Marcus pre-exponential factor, featuring the spin-orbit coupling,  $V_{SO}$ , we replaced the exponential term in equation 6 with that used in Eyring equation (Eq. 9).  $\Delta^\ddagger G$  is estimated from energies almost equally overestimated at the DFT level. This modified expression is employed in Table 1 to compute the kinetic and activation parameters. It performs remarkably well, yielding activation parameters that are very close to the experimental values (88.3 vs. 88.6  $kJ \cdot mol^{-1}$  for the enthalpy and  $-53$  vs.  $-50.2 J \cdot mol^{-1} \cdot K^{-1}$  for the entropy) and to those predicted by WKB theory (90.2  $kJ \cdot mol^{-1}$  and  $-32 J \cdot mol^{-1} \cdot K^{-1}$ ) at a much higher computational cost. Equation 14 therefore offers a faster, more efficient, and simpler route to determine the rate constant (and the associated activation parameters) for the non-adiabatic rotational mechanism.

We have assessed also the influence of the  $S_0/S_1$  mixing in the calculations. To do so, we performed single-point energy calculations with DFT and unrestricted (Broken-Symmetry, BS) DFT at geometries obtained from a SF-TDDFT scan of the singlet ground state. As depicted in Figure 7, there is a perfect match of all three methods close to the *cis* and *trans* minima (green area) and a significant deviation (about 44  $kJ \cdot mol^{-1}$  for DFT and 27  $kJ \cdot mol^{-1}$  for UDFT) only in the TS region (red area). This demonstrates the importance of the SF-TDDFT to take into account the multi-configurational nature of the transition state, which in this case is important due to the strong mixing between the  $S_0$  and  $S_1$  states. Regardless, it is worth stressing that both MECPs between the  $S_0$  and  $T_1$  states are located in the green area of Figure 7, which indicates that one could use single reference methods, such as

classical DFT, to calculate the parameters needed for evaluating the rate constant via the WKB or Marcus equations. With the latter approach, we can derive (see supporting information†) an expression for the transmission coefficient used in Eyring equation,

$$\gamma(T) = \frac{2\pi^{3/2} |V_{SO}|^2}{\sqrt{\lambda k_B^3 T^3}} \quad (15)$$

which is definitely simpler to evaluate than the in WKB formalism (Eq. 8), since we only need the reorganization energy  $\lambda$  and the spin-orbit coupling  $V_{SO}$ . We also tried the Marcus-Levich-Jortner approach to take into account tunneling effects, but this method relies on empirical parameters (i.e., a single effective vibrational mode) which have a strong impact on the kinetic constant so that it is not recommended for quantitative estimates (see supporting information† for more details).

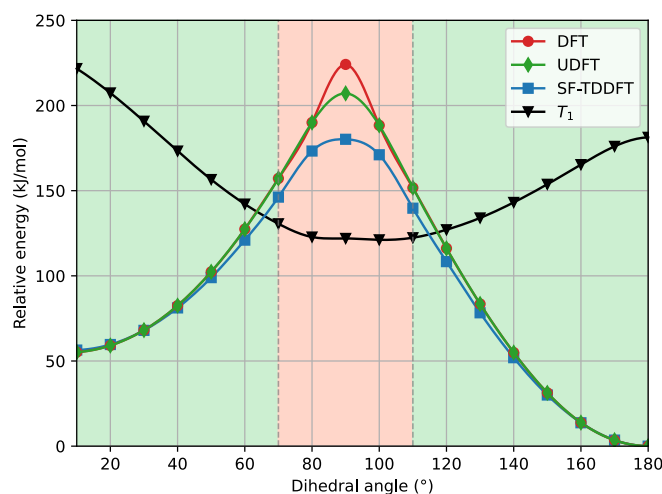


Fig. 7 Single-point energy calculations at the DFT and UDFT level of theory from SF-TDDFT-computed relaxed geometries. In the green area, there is a perfect match between the three methods. In the red area, there is a significant deviation. The  $T_1$  state is represented by the black curve, computed at DFT level of theory. All calculations were performed at the PBE0(D3)/6-311G(d,p) level of theory.

Finally, as a proof of concept, we have applied the proposed methodology to two other azo derivatives: para and meta methoxy-azothiophene (pATH and mATH, respectively), represented in Figure 8. These two heterocyclic azo compounds are of particular interest because they include a thiophene moiety that can be involved in a weak intramolecular interaction between the sulfur atom and the phenyl group on the opposite side of the azo bond, thereby stabilizing the *cis* isomer. These systems were recently described by Martins *et al.*<sup>30</sup> who found, based on CASPT2 calculations, that these two systems will back-isomerize via a mix of non-adiabatic and adiabatic rotations since the inversion pathway is too high in energy. We therefore tracked the inversion and rotation pathways and reported the calculated activation parameters in Table 2; they are found to be in good agreement with the results in reference<sup>30</sup>. Indeed, based on Table 2, the spin-flip PBE0(D3BJ) reproduces well the CASPT2



	Non-adiabatic rotation						Rotation		Inversion	
	WKB (Eq. 8)		Marcus (Eq. 6)		Adapted Marcus (Eq. 14)		Eyring (Eq. 9)		Eyring (Eq. 9)	
	$\Delta^\ddagger H$	$\Delta^\ddagger S$	$\Delta^\ddagger H$	$\Delta^\ddagger S$	$\Delta^\ddagger H$	$\Delta^\ddagger S$	$\Delta^\ddagger H$	$\Delta^\ddagger S$	$\Delta^\ddagger H$	$\Delta^\ddagger S$
CASPT2	78.9	-39	70	-31	82.0	-53	<u>100.5</u>	<u>-13.5</u>	<u>126.7</u>	<u>2.1</u>
PBE0(D3BJ)	90.2	-32	59.3	-45	88.3	-53	124.2	-27	119.2	4.9
MP2	/	/	/	/	/	/	/	/	137.1	16.9
$k$ (298K)	$4.9 \cdot 10^{-5} s^{-1}$		$9.8 \cdot 10^{-1} s^{-1}$			$4.4 \cdot 10^{-6} s^{-1}$	$4.0 \cdot 10^{-11} s^{-1}$		$1.4 \cdot 10^{-8} s^{-1}$	
$\gamma$ (298K)	$4.98 \cdot 10^{-2}$		$1.5 \cdot 10^{-2}$			$8.35 \cdot 10^{-3}$	1		1	
Experimental <sup>16</sup>	88.6	-50.2	$k = 8.5 \cdot 10^{-6} s^{-1}$							
t.b.e <sup>10</sup>	95 ± 4	-38 ± 2	/	/	/	/	118 ± 7	-8	124 ± 3	11

Table 1 Activation parameters for the Z→E isomerization calculated with the WKB or Marcus expression for the non-adiabatic rotation and with the Eyring equation for classical rotation and inversion. Enthalpies are in  $kJ \cdot mol^{-1}$  and entropies in  $J \cdot mol^{-1} \cdot K^{-1}$ . Underlined values are taken from ref<sup>14</sup>, t.b.e (*Theoretical best estimate*), was calculated in ref<sup>10</sup> as the arithmetic average of CCSDT, CCSDT(Q) and MRCI+Q energies. The values of  $k$  and  $\gamma$  were calculated at 298K using the SF-PBE0(D3BJ) approach for each mechanism. The value of  $\lambda$ , used in Marcus equation, was calculated to be  $\lambda = 119 kJ/mol$ .

results for the non-adiabatic and adiabatic rotations. However, there is a non-negligible difference for the inversion mechanism (about  $10 kJ \cdot mol^{-1}$ ), which can compete as well in our case; note that our calculated activation entropies for the inversion mechanism are closer to the experimental ones. Regarding the inversion terms, we observed that this mechanism preferentially occurs on the side of the azo double bond bearing the thiophene substituent (see supporting information†), however we feel more cautious about the individuation of the actually prevailing mechanism, since all enthalpies terms are close, but still the non-adiabatic rotation appears to be the minimum-energy path. It should also be kept in mind that if the mechanisms exhibit similar  $\Delta^\ddagger G$  values, the adiabatic pathways will always be the fastest. One should also consider that the experimental values were obtained in acetonitrile, which is a polar solvent that might thus strongly influence the kinetics of the back-isomerization process. A more expensive approach (e.g. QMMM) could provide further information on how solvents affect the mechanisms. We also suggest an experimental investigation of the heavy-atom effect to obtain information on whether a triplet state is involved or not in the actual mechanism.

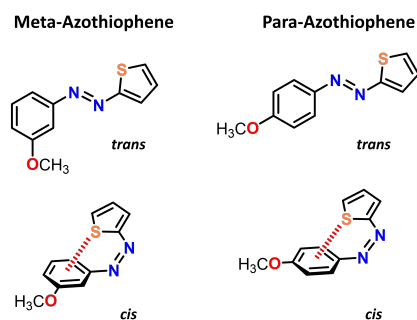


Fig. 8 Chemical structures of meta-methoxy-azothiophene (mAth, left) and of para-methoxy-azothiophene (pAth, right).

## Conclusions

The thermal back-isomerization of *cis* azobenzene is more complex than it firstly appears, since, although the inversion mechanism is well described using conventional DFT, the rotation mechanism exhibits pronounced multiconfigurational character around  $90^\circ$ , where the  $S_0$  and  $S_1$  states strongly mix. Moreover, the emergence of a biradical character might lead to the involvement of a triplet state along the process. We found that the PBE0 functional with the D3BJ empirical dispersion and the 6-311G(d,p) basis set can reproduce highly correlated CASPT2 results by employing the SF-TDDFT formalism. This technique appears to be a powerful tool, as it reproduces highly correlated results in a shorter time. Subsequently, we showed that the Marcus equation can be used by considering the exponential term as described in the Eyring equation, which accounts for the activation energy (in our case, the energy required to reach the MECP), and keeping the actual pre-exponential factor of Marcus equation. We obtain very accurate activation parameters ( $88.3 kJ \cdot mol^{-1}$  and  $-53 J \cdot mol^{-1} \cdot K^{-1}$ ), in excellent agreement with experimental data ( $88.6 kJ \cdot mol^{-1}$  and  $-50.2 J \cdot mol^{-1} \cdot K^{-1}$ ), which represents a major advance for the description of reaction mechanisms in azo compounds. Finally, we reproduced activation parameters for azothiophene derivatives as a proof of concept. This work is a first step towards exploring larger systems than azobenzene for the future, in order to understand how the molecular structure impacts the back isomerization kinetics.

## Author contributions

**Ari Serez:** Writing - Original Draft, Validation, Methodology, Investigation, Conceptualization. **Flavia Aleotti:** Methodology, Writing - Review & Editing. **Pascal Gerbaux:** Writing - Review & Editing, Supervision, Project administration, Funding acquisition. **Luca Muccioli:** Writing - Review & Editing, Methodology. **Jérôme Cornil:** Conceptualization, Writing - Review & Editing, Methodology, Supervision, Project administration, Funding acquisition.



	Non-adiabatic rotation				Rotation		Inversion	
	WKB (Eq. 8)		Marcus (Eq. 14)		Eyring (Eq. 9)		Eyring (Eq. 9)	
	$\Delta^\ddagger H$	$\Delta^\ddagger S$	$\Delta^\ddagger H$	$\Delta^\ddagger S$	$\Delta^\ddagger H$	$\Delta^\ddagger S$	$\Delta^\ddagger H$	$\Delta^\ddagger S$
CASPT2 (pAth) <sup>30</sup>	92.1	-39.7	/	/	105.3	-0.6	135.1	-0.2
CASPT2 (mAth) <sup>30</sup>	97.2	-43.2	/	/	111.8	0.2	138.1	-0.1
SF (pAth)	90.8	-32.0	88.4	-56.2	115.5	-4.9	100.0	-7.5
SF (mAth)	95.0	-31.0	92.4	-55.5	123.5	17.32	102.2	-2.9
$k$ (298K, pAth)	$1.4 \cdot 10^{-5}$		$2.38 \cdot 10^{-6}$		$1.9 \cdot 10^{-8}$		$7.3 \cdot 10^{-6}$	
$k$ (298K, mAth)	$2.9 \cdot 10^{-6}$		$6.35 \cdot 10^{-7}$		$1.1 \cdot 10^{-8}$		$5.2 \cdot 10^{-6}$	
$\gamma$ (298K, pAth)	$3.5 \cdot 10^{-2}$		$5.8 \cdot 10^{-3}$		1		1	
$\gamma$ (298K, mAth)	$3.8 \cdot 10^{-2}$		$6.3 \cdot 10^{-3}$		1		1	
Exp. <sup>33</sup> (pAth)	86.6	-12.5	$k = 3.9 \cdot 10^{-6}$					
Exp. <sup>33</sup> (mAth)	96.2	-12.5	$k = 3.2 \cdot 10^{-7}$					

Table 2 Activation parameters calculated with WKB and the adapted Marcus equations for the non-adiabatic rotation and with Eyring equation for classical rotation and inversion. SF stands for "Spin-Flip", meaning SF-TDDFT evaluated at PBE0(D3BJ)/6-311G(d,p). Enthalpies are in  $\text{kJ} \cdot \text{mol}^{-1}$ , entropies in  $\text{J} \cdot \text{mol}^{-1} \cdot \text{K}^{-1}$  and rate constants in  $\text{s}^{-1}$ . We calculated the value of  $\lambda$  for each structure:  $\lambda_{\text{pAth}} = 135 \text{ kJ/mol}$ ,  $\lambda_{\text{mAth}} = 138 \text{ kJ/mol}$ . The value of the spin-orbit coupling is the following:  $V_{\text{SO}}(\text{pAth}) = 13.5 \text{ cm}^{-1}$ ,  $V_{\text{SO}}(\text{mAth}) = 12.9 \text{ cm}^{-1}$ . The values of  $k$  and  $\gamma$  were calculated at 298K using the SF-PBE0(D3BJ) approach for each mechanism.

sition.

## Conflicts of interest

There are no conflicts to declare.

## Data availability

The data supporting this study are available from the corresponding author upon request.

## Acknowledgements

A.S. is supported by the Action de Recherche Concertée (ARC) program funded by UMONS on "MOlecular Solar Thermal systems: from molecules to energy capture/exchange prototypes". The work in Mons has also been supported by the Fund for Scientific Research (FRS) of FNRS within the Consortium des Equipements de Calcul Intensif (CECI) under grant 2.5020.11 and by the Walloon Region (LUCIA Tier-1 supercomputer) under grant 1117545. J.C. is an FNRS research director. F.A. and L.M. acknowledge funding awarded by the International Foundation Big Data and Artificial Intelligence for Human Development (IFAB) to the project "Getting the MOST out of Sun" (GEM).

## Notes and references

- H. M. Bandara and S. C. Burdette, *Chemical Society Reviews*, 2012, **41**, 1809–1825.
- K. Börjesson, A. Lennartson and K. Moth-Poulsen, *ACS Sustainable Chemistry and Engineering*, 2013, **1**, 585–590.
- W. Sun, Z. Shangguan, X. Zhang, T. Dang, Z. Y. Zhang and T. Li, *ChemSusChem*, 2023, **16**, 1–8.
- Z. Wang, P. Erhart, T. Li, Z. Y. Zhang, D. Sampedro, Z. Hu, H. A. Wegner, O. Brummel, J. Libuda, M. B. Nielsen and K. Moth-Poulsen, *Joule*, 2021, **5**, 3116–3136.
- K. Moth-Poulsen, D. C'oso, K. Börjesson, N. Vinokurov, S. K. Meier, A. Majumdar, K. P. C. Vollhardt and R. A. Segalman, *Energy and Environmental Science*, 2012, **5**, 8534–8537.
- L. Dong, Y. Feng, L. Wang and W. Feng, *Chemical Society Reviews*, 2018, **47**, 7339–7368.
- Z. Wang, H. Hölzel and K. Moth-Poulsen, *Chemical Society Reviews*, 2022, **51**, 7313–7326.
- Z. Zhang, W. Wang, M. O'Hagan, J. Dai, J. Zhang and H. Tian, *Angewandte Chemie - International Edition*, 2022, **61**, 1–24.
- A. Cembran, F. Bernardi, M. Garavelli, L. Gagliardi and G. Orlandi, *Journal of the American Chemical Society*, 2004, **126**, 3234–3243.
- M. Reimann, E. Teichmann, S. Hecht and M. Kaupp, *Journal of Physical Chemistry Letters*, 2022, **13**, 10882–10888.
- S. Axelrod, E. Shakhnovich and R. Gómez-Bombarelli, *ACS Central Science*, 2023, **9**, 166–176.
- J. Calbo, C. E. Weston, A. J. White, H. S. Rzepa, J. Contreras-García and M. J. Fuchter, *Journal of the American Chemical Society*, 2017, **139**, 1261–1274.
- T. Robert, G. Henrard, B. Tassignon, A. Serez, J. De Winter, P. Dugourd, J. Cornil, F. Chirot and P. Gerbault, *Analytical Chemistry*, 2025, **97**, 9405–9413.
- F. Aleotti, L. Soprani, L. F. Rodríguez-Almeida, F. Calcagno, F. Loprete, I. Rivalta, S. Orlandi, E. Canè, M. Garavelli, I. Conti and L. Muccioli, *Molecular Systems Design and Engineering*, 2024.
- C. R. Crecca and A. E. Roitberg, *Journal of Physical Chemistry A*, 2006, **110**, 8188–8203.
- T. Asano, T. Okada, S. Shinkai, K. Shigemats, Yumiko K and O. Manabe, *J. Am. Chem. Soc.*, 1981, **103**, 5161–5165.



- 17 C. Rietze, E. Titov, S. Lindner and P. Saalfrank, *Journal of Physics Condensed Matter*, 2017, **29**, 314002–314024.
- 18 C. M. Marian, *Wiley Interdisciplinary Reviews: Computational Molecular Science*, 2012, **2**, 187–203.
- 19 D. Casanova and A. I. Krylov, *Physical Chemistry Chemical Physics*, 2020, **22**, 4326–4342.
- 20 S. Tsuzuki and T. Uchimaru, *Physical Chemistry Chemical Physics*, 2020, **22**, 22508–22519.
- 21 J. N. Harvey, *Physical Chemistry Chemical Physics*, 2007, **9**, 331–343.
- 22 E. J. Piechota and G. J. Meyer, *Journal of Chemical Education*, 2019, **96**, 2450–2466.
- 23 S. Liu, S. Srinivasan, J. Tao, M. C. Grady, M. Soroush and A. M. Rappe, *Journal of Physical Chemistry A*, 2014, **118**, 9310–9318.
- 24 A. O. Lykhin, D. S. Kaliakin, G. E. Depolo, A. A. Kuzubov and S. A. Varganov, *International Journal of Quantum Chemistry*, 2016, **116**, 750–761.
- 25 G. F. Bertsch, *Derivations of Marcus's formula*, <https://archive.int.washington.edu/users/bertsch/marcus.1.pdf>.
- 26 K. L. Gannon, M. A. Blitz, C. H. Liang, M. J. Pilling, P. W. Seakins, D. R. Glowacki and J. N. Harvey, *Faraday Discussions*, 2010, **147**, 173–188.
- 27 S. Kotaru, P. Pokhilko and A. I. Krylov, *Journal of Chemical Physics*, 2022, **157**, 224110.
- 28 Y. Shao, Z. Gan, E. Epifanovsky, A. T. Gilbert, M. Wormit, J. Kussmann, A. W. Lange, A. Behn, J. Deng, X. Feng, D. Ghosh, M. Goldey, P. R. Horn, L. D. Jacobson, I. Kaliman, R. Z. Khaliullin, T. Kus, A. Landau, J. Liu, E. I. Proynov, Y. M. Rhee, R. M. Richard, M. A. Rohrdanz, R. P. Steele, E. J. Sundstrom, H. L. Woodcock, P. M. Zimmerman, D. Zuev, B. Albrecht, E. Alguire, B. Austin, G. J. Beran, Y. A. Bernard, E. Berquist, K. Brandhorst, K. B. Bravaya, S. T. Brown, D. Casanova, C. M. Chang, Y. Chen, S. H. Chien, K. D. Closser, D. L. Crittenden, M. Diedenhofen, R. A. Distasio, H. Do, A. D. Dutoi, R. G. Edgar, S. Fatehi, L. Fusti-Molnar, A. Ghysels, A. Golubeva-Zadorozhnaya, J. Gomes, M. W. Hanson-Heine, P. H. Harbach, A. W. Hauser, E. G. Hohenstein, Z. C. Holden, T. C. Jagau, H. Ji, B. Kaduk, K. Khistyayev, J. Kim, J. Kim, R. A. King, P. Klunzinger, D. Kosenkov, T. Kowalczyk, C. M. Krauter, K. U. Lao, A. D. Laurent, K. V. Lawler, S. V. Levchenko, C. Y. Lin, F. Liu, E. Livshits, R. C. Lochan, A. Luenser, P. Manohar, S. F. Manzer, S. P. Mao, N. Mardirossian, A. V. Marenich, S. A. Maurer, N. J. Mayhall, E. Neuscamman, C. M. Oana, R. Olivares-Amaya, D. P. O'Neill, J. A. Parkhill, T. M. Perrine, R. Peverati, A. Prociuk, D. R. Rehn, E. Rosta, N. J. Russ, S. M. Sharada, S. Sharma, D. W. Small, A. Sodt, T. Stein, D. Stück, Y. C. Su, A. J. Thom, T. Tsuchimochi, V. Vanovschi, L. Vogt, O. Vydrov, T. Wang, M. A. Watson, J. Wenzel, A. White, C. F. Williams, J. Yang, S. Yeganeh, S. R. Yost, Z. Q. You, I. Y. Zhang, X. Zhang, Y. Zhao, B. R. Brooks, G. K. Chan, D. M. Chipman, C. J. Cramer, W. A. Goddard, M. S. Gordon, W. J. Hehre, A. Klamt, H. F. Schaefer, M. W. Schmidt, C. D. Sherrill, D. G. Truhlar, A. Warshel, X. Xu, A. Aspuru-Guzik, R. Baer, A. T. Bell, N. A. Besley, J. D. Chai, A. Dreuw, B. D. Dunietz, T. R. Furlani, S. R. Gwaltney, C. P. Hsu, Y. Jung, J. Kong, D. S. Lambrecht, W. Liang, C. Ochsenfeld, V. A. Rassolov, L. V. Slipchenko, J. E. Subotnik, T. Van Voorhis, J. M. Herbert, A. I. Krylov, P. M. Gill and M. Head-Gordon, *Molecular Physics*, 2015, **113**, 184–215.
- 29 M. Huix-Rotllant, B. Natarajan, A. Ipatov, C. Muhavini Wawire, T. Deutsch and M. E. Casida, *Physical Chemistry Chemical Physics*, 2010, **12**, 12811–12825.
- 30 F. A. Martins, R. V. Viesser, J. V. Schober, R. Herges and J. I. Wu, *Journal of the American Chemical Society*, 2025.
- 31 D. Beljonne, Z. Shuai, G. Pourtois and J. L. Bredas, *Journal of Physical Chemistry A*, 2001, **105**, 3899–3907.
- 32 C. J. Cramer, *Essentials of Computational Chemistry Theories and Models Second Edition*, Wiley, 2nd edn, 2004, pp. 1–624.
- 33 A. H. Heindl and H. A. Wegner, *Chemistry - A European Journal*, 2020, **26**, 13730–13737.



The data supporting this study are available from the corresponding author upon request.

